# Thermoluminescence Study of Persistent Luminescence Materials: $Eu^{2+}$- and $R^{3+}$-Doped Calcium Aluminates, $CaAl_2O_4:Eu^{2+},R^{3+}$

**Tuomas Aitasalo,[†,‡] Jorma Hölsä,[†] Högne Jungner,[§] Mika Lastusaari,[†] and Janne Niittykoski*[,†,‡]**

*Department of Chemistry, University of Turku, FI-20014 Turku, Finland, Graduate School of Materials Research, Turku, Finland, and Dating Laboratory, University of Helsinki, P.O. Box 64, FI-00014, Helsinki, Finland*

*Received: December 9, 2005; In Final Form: January 10, 2006*

Thermoluminescence properties of the $Eu^{2+}$-, $R^{3+}$-doped calcium aluminate materials, $CaAl_2O_4:Eu^{2+},R^{3+}$, were studied above room temperature. The trap depths were estimated with the aid of the preheating and initial rise methods. The seemingly simple glow curve of $CaAl_2O_4:Eu^{2+}$ peaking at ca. 80 °C was found to correspond to several traps. The $Nd^{3+}$ and $Tm^{3+}$ ions, which enhance most the intensity of the high-temperature TL peaks, form the most suitable traps for intense and long-lasting persistent luminescence, too. The location of the 4f and 5d ground levels of the $R^{3+}$ and $R^{2+}$ ions were deduced in relation to the band structure of $CaAl_2O_4$. No clear correlation was found between the trap depths and the $R^{3+}$ or $R^{2+}$ level locations. The traps may thus involve more complex mechanisms than the simple charge transfer to (or from) the $R^{3+}$ ions. A new persistent luminescence mechanism presented is based on the photoionization of the electrons from $Eu^{2+}$ to the conduction band followed by the electron trapping to an oxygen vacancy, which is aggregated with a calcium vacancy and a $R^{3+}$ ion. The migration of the electron from one trap to another and also to the aggregated $R^{3+}$ ion forming $R^{2+}$ (or $R^{3+}-e^-$) is then occurring. The reverse process of a release of the electron from traps to $Eu^{2+}$ will produce the persistent luminescence. The ability of the $R^{3+}$ ions to trap electrons is probably based on the different reduction potentials and size of the $R^{3+}$ ions. Hole trapping to a calcium vacancy and/or the $R^{3+}$ ion may also occur. The mechanism presented can also explain why $Na^+$, $Sm^{3+}$, and $Yb^{3+}$ suppress the persistent luminescence.

## 1. Introduction

The long afterglow (i.e., persistent luminescence) exhibited by some phosphors is usually considered as a harmful feature for conventional applications such as scintillators or cathode ray tubes.[1] However, for certain applications, e.g., luminous paints, the persistent luminescence is essential.[2] The material used so far, ZnS doped with copper (and codoped with cobalt), is extremely sensitive to moisture and thus is chemically unstable. The persistent luminescence of ZnS:Cu,Co is initially rather strong but is limited only to a few hours, too. As a result, ZnS:Cu,Co needs an additional excitation source since the energy storage capacity of the material is not sufficient. Radioactive nuclei ($^3H$, $^{147}Pm$) have been used to provide this additional excitation but are no longer acceptable. Stable, efficient and nonradioactive materials replacing ZnS:Cu,Co are thus urgently needed due to, e.g., environmental reasons.

The alkaline earth aluminates doped with $Eu^{2+}$ and rare earth ($R^{3+}$) ions, $MAl_2O_4:Eu^{2+},R^{3+}$ (M = Ca and Sr) are at present the best candidates to replace the outdated ZnS:Cu,Co as commercial persistent luminescence materials.[3−9] It has been presented that the persistent luminescence of $MAl_2O_4:Eu^{2+}$ is strongly enhanced by codoping with selected trivalent rare earth ions, e.g., $Dy^{3+}$ and $Nd^{3+}$.[10−12] It is evident that the $Eu^{2+}$ ion acts as a luminescent center emitting in the blue ($\lambda_{max}$ = 440 nm) and green (520 nm) spectral range for $CaAl_2O_4:Eu^{2+}$ and $SrAl_2O_4:Eu^{2+}$, respectively. Much less agreement exists on the role of the $R^{3+}$ codopant. The $R^{3+}$ ion has been assumed to act as a trap or at least to modify the trap properties in these phosphors. Although a massive number of studies dealing with the phenomenon has already been published, the mechanism of the persistent luminescence obtained from the $MAl_2O_4:Eu^{2+},R^{3+}$ materials has not been elucidated. Theories that have been presented up to date, e.g., refs 10−17, are often contradictory. One reason for this uncertainty can be the fact that the original persistent luminescence of $MAl_2O_4:Eu^{2+}$ has almost entirely been forgotten and research has been concerted only to those materials, $CaAl_2O_4:Eu^{2+},Nd^{3+}$ and $SrAl_2O_4:Eu^{2+},Dy^{3+}$, which yield the best persistent luminescence.

New applications for the persistent luminescence materials have been presented lately, such as radiation detection[18] as well as sensors for structural damage, fracture of materials,[19−21] and temperature.[22] These applications demand the exact knowledge of the luminescence mechanisms and the trap identification. The development of new materials would also be greatly facilitated if the mechanisms were known.

Measurement of the thermoluminescence (TL) glow curves is one of the most useful ways to determine the number as well as the activation energy of the trapping levels in materials.[23] The low temperature thermoluminescence study[24] of $CaAl_2O_4:Eu^{2+},R^{3+}$ revealed several groups of $R^{3+}$ ions which

* Corresponding author. Fax: +358-2-3336700. E-mail: japeni@utu.fi.
† University of Turku.
‡ Graduate School of Materials Research.
§ University of Helsinki.

10.1021/jp057185m CCC: $33.50 
Published on Web 02/22/2006

have rather different effects on TL and persistent luminescence though most $R^{3+}$ ions were observed to reduce the low temperature thermoluminescence of $CaAl_2O_4:Eu^{2+}$. Only a few rare earth ions ($Nd^{3+}$ and $Tm^{3+}$) caused intense and long-lasting persistent luminescence when codoped into $CaAl_2O_4:Eu^{2+}$. The low-temperature TL measurements did not, however, reveal the presence of deep traps (i.e., high-temperature TL peaks above 50 °C), which can affect the persistent luminescence. In particular, the TL peaks close to (or above) the room temperature are expected to be essential to the persistent luminescence. When applications as radiation detection are considered, the deep traps, and the identification of them, are the most important issues. Since the low temperature TL glow curves were observed to depend significantly on the individual $R^{3+}$ ion, there is no doubt that the high-temperature TL glow curves could be affected in a similar manner.

In the present work, the high-temperature TL measurements of calcium aluminate materials doped with $Eu^{2+}$ and codoped with $R^{3+}$ ($Y^{3+}$, $La^{3+}-Lu^{3+}$, excluding $Pm^{3+}$ and $Eu^{3+}$), $CaAl_2O_4:Eu^{2+},R^{3+}$, were carried out between 25 and 400 °C. The trap depths and densities in these materials were derived from the TL glow curves. The nature of trapping levels in $CaAl_2O_4:Eu^{2+}$ as well as the effect of the $R^{3+}$ ion codoping on the thermoluminescence and persistent luminescence of these materials were discussed in view of the results obtained. The reasons for the performance of the best blue emitting persistent luminescence material up to date, $CaAl_2O_4:Eu^{2+},Nd^{3+}$, were assessed. Finally, a new persistent luminescence mechanism is proposed.

## 2. Experimental Section

**2.1. Materials Preparation.** The polycrystalline $Eu^{2+}$-doped and $R^{3+}$-codoped calcium aluminates ($CaAl_2O_4:Eu^{2+},R^{3+}$) were prepared by annealing the stoichiometric amounts of calcium carbonate ($CaCO_3$), aluminum oxide ($Al_2O_3$), europium oxide ($Eu_2O_3$, 0.5 mol %) and rare earth oxide (usually $R_2O_3$, 1 mol %), with boron oxide ($B_2O_3$, 1 mol %) as a flux in a reducing ($N_2$ + 12% $H_2$, flow rate: 10 $cm^3$ $min^{-1}$) atmosphere at 1250 °C for 6 h. A complementary $CaAl_2O_4:Eu^{3+}$ ($Eu_2O_3$, 0.5 mol %) material was prepared by annealing previously prepared $CaAl_2O_4:Eu^{2+}$ in air at 1100 °C for 20 h. The phase and structural purity of the materials was routinely checked by using the X-ray powder diffraction methods but additional phases were not observed.

**2.2. Luminescence Measurements.** The UV excited and persistent luminescence spectra of $CaAl_2O_4:Eu^{2+},R^{3+}$ and the time dependence of the latter as well as the excitation spectrum of $CaAl_2O_4:Eu^{3+}$ were measured at room temperature with a Perkin-Elmer LS-5 spectrometer. The excitation ($\lambda_{exc}$ = 350 nm) source was a xenon lamp. Prior to the persistent luminescence measurements, the materials were irradiated with a conventional (11 W Osram Dulux S) tricolor fluorescent tube for 5 min. Time-resolved luminescence was measured at room temperature using a Xe lamp ($\lambda_{exc}$ = 250 nm, dispersed through a Jobin Yvon DH10 monochromator) excitation and a Hamamatsu R4220 photomultiplier detection. The VUV/UV experiments were carried out at the SUPERLUMI station of HASYLAB at DESY (Hamburg, Germany) under pulsed excitation by 50−320 nm synchrotron radiation from the DORIS storage ring. For the measurement of the excitation spectra the luminescence was detected by a Hamamatsu R6358P photomultiplier.

**2.3. Thermoluminescence Measurements.** Thermoluminescence glow curves were measured with a Risø TL/OSL-DA-12 system in the temperature range from 25 to 400 °C operating with linear heating rates of 2, 4, 5, 6, 8, and 10 °C $s^{-1}$. The global TL emission from UV to 650 nm was monitored. Prior to the TL measurements, the materials were exposed to the radiation from a conventional 20 W incandescent lamp. The irradiation time was varied from 5 to 240 s. The short irradiation times were chosen to avoid photomultiplier saturation due to the intense thermoluminescence of the materials. The traps are probably only partially filled as a result of this short exposure. A delay of 3 min was employed between the end of irradiation and the actual TL measurement. The sample weight was kept constant (10 mg). The TL intensities are thus comparable. Other factors (e.g., sample packing and position), which are very difficult to control, may, however, induce error for the TL intensity.

**2.4. Preheating and Initial Rise Methods.** The preheating method[23] was used to study the number of traps in detail. After the irradiation, the materials were first heated to a temperature ($T_{stop}$) and then rapidly cooled to room temperature. Thereafter the TL experiment was carried out using the heating rate of 5 °C $s^{-1}$. This procedure was repeated for the $T_{stop}$ values between 50 and 250 °C in steps of 5 °C. The preheating method reveals usually only the strongest peaks. The TL peak positions obtained by this method are usually higher than the actual positions because of a peak overlap. The resolution of the technique has been estimated to be ca. 5 °C.[23]

The initial rise method[23] was used to determine the trap depths ($E$) from the preheated glow curves. In the beginning of the glow curve, the thermoluminescence intensity ($I$) is, irrespective of the kinetic order, exponentially dependent on temperature (eq 1):

$$I = \text{constant} \times \exp\left(-\frac{E}{kT}\right) \tag{1}$$

where $k$ is the Boltzmann constant. $E$ can be found from the slope of the straight line obtained by plotting $\ln(I)$ against $1/T$. The temperature range used for the analysis was restricted in such a way that the thermoluminescence intensity did not exceed 15% of the peak maximum temperature.

The lifetime ($\tau$) of the charge carriers in traps can be estimated in an approximate manner from the calculated trap depths at any temperature (eq 2):

$$\tau = s^{-1} \times \exp\left(-\frac{E}{kT}\right) \tag{2}$$

where $s$ is the frequency factor.

**2.5. Energy Level Location of Rare Earth Ions.** To predict the ability of the rare earth ions to trap electrons or holes, the location of the 4f and 5d ground levels of both the $R^{2+}$ and $R^{3+}$ ions relative to the conduction and valence band in $CaAl_2O_4$ should be estimated. The method developed by P. Dorenbos[25−27] was used in this work. The energy for the first 4f → 5d transition ($E_{fd}$) of the $R^{n+}$ ion in a compound A is obtained by eq 3:[25]

$$E_{fd}(R^{n+},A) = E_{Afree}(R^{n+}) - D(R^{n+},A) \tag{3}$$

where $E_{Afree}(R^{n+})$ are constants averaged over 300 compounds with values close to those of the first 4f → 5d transition energies of the free $R^{n+}$ ions ($E_{fd,free}$). The redshift $D(R^{n+},A)$ is the amount by which the 5d level is shifted toward lower energy when compared to the free ion, when the rare earth ion is embedded in a compound A. The $Ce^{3+}$ ion for which spectro-

scopic data is abundant, is used as a reference for the $R^{3+}$ ions (eq 4):

$$E_{\text{Afree}}(R^{3+}) = E_{\text{fd,free}}(Ce^{3+}) + E_{\text{fd}}(R^{3+},A) - E_{\text{fd}}(Ce^{3+},A) \quad (4)$$

In the same way and for the same reason, the $Eu^{2+}$ ion is used as a reference for the $R^{2+}$ ions. In the $R^{2+}$ (and $R^{3+}$) series, the redshift is within 0.1 eV the same for all $R^{n+}$ ions when embedded in the same site and the same compound. Tabulated $D(R^{n+},A)$ values can be found in the literature for the $R^{2+}$ [28] and $R^{3+}$ [29] ions.

The 4f ground level location of the $R^{2+}$ ions can now be estimated, since the charge-transfer energy ($E_{CT}$) of $R^{3+}$ can be depicted as a direct measure for the energy difference between the top of the valence band and the 4f ground level ($E_{Vf}$) of the $R^{2+}$ ions in a compound A.[25] When $\Delta E_{CT}(R^{3+})$ is defined as the average energy difference of CT to $R^{3+}$ (and to $Eu^{3+}$) then (eq 5):

$$E_{Vf}(R^{2+},A) \approx E_{CT}(R^{3+},A) = E_{CT}(Eu^{3+},A) + \Delta E_{CT}(R^{3+}) \approx E_{CT}(Eu^{3+},A) + \Delta E_{Vf}(R^{2+}) \quad (5)$$

The energies $\Delta E_{Vf}(R^{2+})$ are host compound independent constants which can be found in the literature.[25] The $E_{Vf}$ energies of $R^{2+}$ ions are inversely proportional to the 3rd ionization potentials of rare earths, since the most stable trivalent (Gd) and divalent (Eu) ions have low and high potentials, respectively.[30]

The energy difference between the valence band and the lowest 5d level ($E_{Vd}$) of the $R^{2+}$ ion can be estimated with the aid of $E_{CT}(Eu^{3+})$ and $E_{fd}(Eu^{2+})$ (eq 6):[25]

$$E_{Vd}(R^{2+},A) = E_{CT}(Eu^{3+},A) + E_{fd}(Eu^{2+},A) + \Delta E_{Vd}(R^{2+}) \quad (6)$$

where $\Delta E_{Vd}(R^{2+}) = E_{Vd}(R^{2+}) - E_{Vd}(Eu^{2+}) = \Delta E_{Vf}(R^{2+}) + E_{\text{Afree}}(R^{2+}) - E_{\text{Afree}}(Eu^{2+})$. The $\Delta E_{Vd}(R^{2+})$ values can be found in the literature.[25] $E_{fd}(Eu^{2+},A)$ is the energy difference between the lowest 5d level and the 4f ground level for a compound A. This energy can be estimated from the lowest band position in excitation or luminescence spectra. The luminescence band is due to the relaxed 5d level, which is shifted ca. 0.1−0.5 eV to lower energy (i.e., Stokes shift) compared to the lowest band in the excitation spectrum.[31] In relation to the host band structure, the lowest 5d level location is almost constant from $La^{2+}$ to $Eu^{2+}$ but increases by 0.6 eV from $Eu^{2+}$ to $Yb^{2+}$.[25] The different 4f → 5d energies for the $R^{2+}$ ions are thus due to the different location of the 4f ground level.

The energy level locations for the $R^{3+}$ ions can be constructed with techniques similar to those used for the $R^{2+}$ ions.[26] However, there is not much information about the charge-transfer energies for $Ce^{4+}$ (or any other $R^{4+}$) in order to define the 4f ground level position of the $R^{3+}$ ions. Therefore, other data must be used, e.g., the photoionization (energy difference from the 5d level to the conduction band) or photoconduction (energy difference from the 4f ground level to the conduction band) energies for $R^{3+}$, usually $Ce^{3+}$. The $E_{Vf}$ energies of $R^{3+}$ ions are inversely proportional to the 4th ionization potentials of rare earths, since the most stable trivalent (Gd) and tetravalent (Ce) ions have high and low potentials, respectively.[30]

As a conclusion, the entire system of the 4f and 5d ground level locations of both the $R^{2+}$ and $R^{3+}$ ions in relation to the host band structure can be constructed with the aid of the eqs 5 and 6. Additional experimental data is needed, however: the band gap energy of the host compound, the CT energy of one $R^{3+}$ ($Eu^{3+}$), the 5d → 4f emission band position of one $R^{2+}$ ($Eu^{2+}$), as well as the 5d → 4f emission band position and photoionization or photoconduction energy of one $R^{3+}$ ($Ce^{3+}$). If the data only for $R^{2+}$ (or $R^{3+}$) exists, the energy level locations for $R^{3+}$ (or $R^{2+}$) can be approximated as follows (eq 7): [16]

$$E_{fd}(Eu^{2+}) = 0.64 \times E_{fd}(Ce^{3+}) + 0.53 \text{ eV} \quad (7)$$

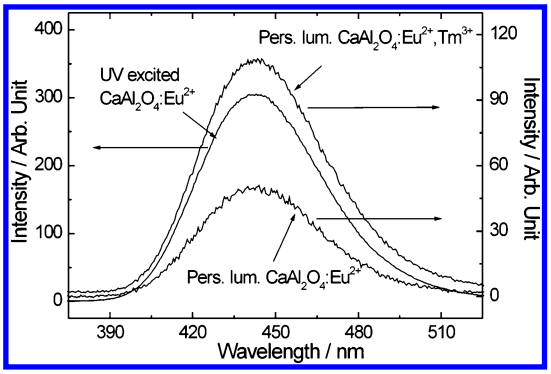


**Figure 1.** UV excited and persistent luminescence spectra of selected $CaAl_2O_4:Eu^{2+},R^{3+}$ materials at room temperature.

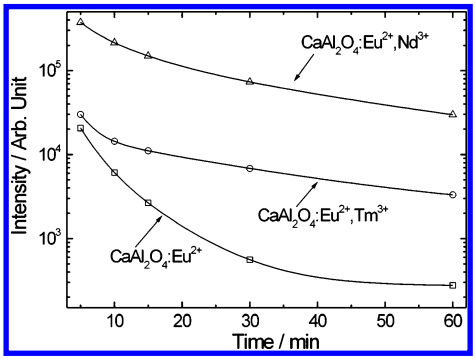


**Figure 2.** Time dependence of persistent luminescence intensity of selected $CaAl_2O_4:Eu^{2+},R^{3+}$ (R = Nd and Tm) materials at room temperature.

## 3. Results and Discussion

**3.1. Thermoluminescence.** The UV excited and persistent luminescence of $Eu^{2+}$-doped $CaAl_2O_4$ was observed in the blue region as one band centered at 440 nm (Figure 1) in good agreement with the previous reports.[4,14] Some $R^{3+}$ ions (e.g., $Nd^{3+}$, $Tm^{3+}$) enhance the persistent luminescence intensity and lengthen the lifetime (Figure 2), but none of them was found to affect the luminescence wavelength or the shape of the spectrum. Therefore, the two emissions can be concluded to originate from the same $Eu^{2+}$ center. No $R^{3+}$ ion or intrinsic defect related emission was observed. In the present work, the thermoluminescence glow curve of $CaAl_2O_4:Eu^{2+}$ was used as a reference to study the effect of the $R^{3+}$ codoping on the properties of traps. Using the heating rate of 5 °C $s^{-1}$ the main TL peak is observed at ca. 80 °C followed by a tail up to 200 °C (Figure 3). The FWHM of the main peak is ca. 40 °C.

**3.2. Effect of $R^{3+}$ Codoping.** The rare earth ions were previously divided into several groups depending on their effect on the low temperature thermoluminescence.[24] The reasons for the different behavior of the $R^{3+}$ ions are still uncertain, however. Because of their rather similar chemical properties, the effect of the $R^{3+}$ ions should be similar and thus the physical properties, mainly the ionization potentials and the 4f and 5d energy levels may play an important role. The effect of the differences in ionic size and bonding characteristics as well as

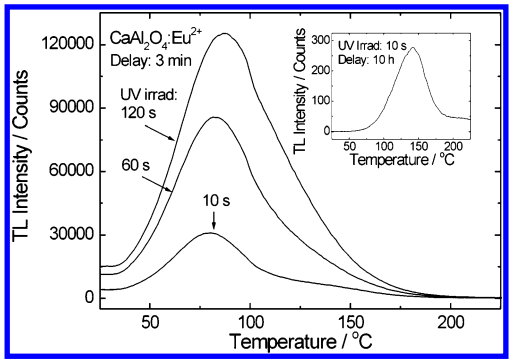


**Figure 3.** Thermoluminescence glow curves of $CaAl_2O_4:Eu^{2+}$ with different irradiation times (delay: 3 min and 10 h, heating rate: 5 °C $s^{-1}$).

**TABLE 1: Thermoluminescence Peak Maxima (in °C) and Intensities (in Normalized Arbitrary Units) of the TL Glow Curves of $CaAl_2O_4:Eu^{2+},R^{3+}$** [a]

| R | $T_1$ | $I_1$ | $T_2$ | $I_2$ | $T_3$ | $I_3$ | total $I$ |
|---|---|---|---|---|---|---|---|
| none | 80 | 100 | 134 | 7 | | | 100 |
| La | 79 | 9 | 133 | 0.8 | | | 8 |
| Ce | 83 | 660 | | | | | 610 |
| Pr | 81 | 150 | | | | | 130 |
| Nd | 95 | 210 | 137 | 210 | | | 370 |
| Sm | 99 | 0.5 | | | 320 | 2 | 1 |
| Gd | 72 | 2 | 125 | 0.9 | | | 3 |
| Tb | 78 | 200 | 118 | 9 | | | 190 |
| Dy | 88 | 110 | 138 | 370 | | | 420 |
| Ho | 83 | 450 | | | | | 390 |
| Er | 76 | 12 | | | | | 12 |
| Tm | | | 115 | 190 | | | 160 |
| Yb | 77 | 3 | 138 | 0.01 | 290 | 0.3 | 3 |
| Lu | 77 | 2 | 126 | 2 | | | 4 |
| Y | 76 | 0.8 | 120 | 0.6 | 272 | 0.5 | 2 |

[a] Numbering of peaks starts from the lowest temperature peak observed. Overlapping peaks were deconvoluted, and the intensities were obtained as the area under the (deconvoluted) peaks.

some redox properties cannot be excluded, however. In the present work, the TL intensities and peak positions are used as the criteria to classify the $R^{3+}$ ions. The data presented (Table 1) are based on the deconvolution of the TL glow curves after visual evaluation. The deconvolution is not a scientifically sound method of interpretation and analysis of TL glow curves and thus does not give the exact band number, maxima or intensities, but helps the reader to compare the effect of the codopants easily.

Roughly speaking, $La^{3+}$, $Sm^{3+}$, $Gd^{3+}$, $Er^{3+}$, $Yb^{3+}$, $Lu^{3+}$, and $Y^{3+}$ have all quite a similar effect: they reduce (by ca. 90%) the overall TL intensity of $CaAl_2O_4:Eu^{2+}$ from 25 to 400 °C (Table 1). These ions weakened also the persistent luminescence and the low-temperature TL.[24] There is thus a clear correlation between the TL and persistent luminescence intensity which can be established with rather simple TL measurements. The effect of some $R^{3+}$ ions ($Gd^{3+}$ and $Er^{3+}$), which create new low-temperature TL peaks corresponding to very shallow traps,[24] explains in a straightforward manner the weak persistent luminescence. The typical trivalent $La^{3+}$, $Gd^{3+}$, $Er^{3+}$, and $Lu^{3+}$ ions weaken TL of $CaAl_2O_4:Eu^{2+}$ (Figure 4), but do not clearly change the glow curve shape or peak positions. The high-temperature tail of the glow curves is, however, more visible due to weak intensity of the main peak. The $Sm^{3+}$, $Yb^{3+}$ (easily reduced), and $Y^{3+}$ ions reduce strongly the TL intensity and yield new weak high-temperature TL peaks (Figure 5).

The materials codoped with the $Ce^{3+}$, $Pr^{3+}$, $Tb^{3+}$ (easily oxidized), and $Ho^{3+}$ ions display a very similar TL main peak

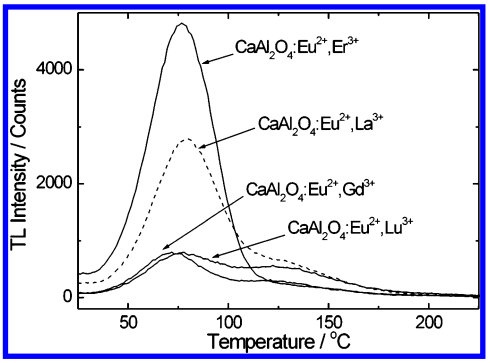


**Figure 4.** Thermoluminescence glow curves of $CaAl_2O_4:Eu^{2+},R^{3+}$ (R = La, Gd, Er and Lu; irradiation time, 10 s; heating rate, 5 °C $s^{-1}$).

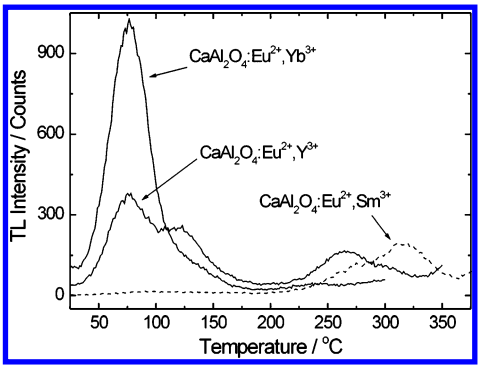


**Figure 5.** Thermoluminescence glow curves of $CaAl_2O_4:Eu^{2+},R^{3+}$ (R = Sm, Yb, and Y; irradiation time, 10 s; heating rate, 5 °C $s^{-1}$).

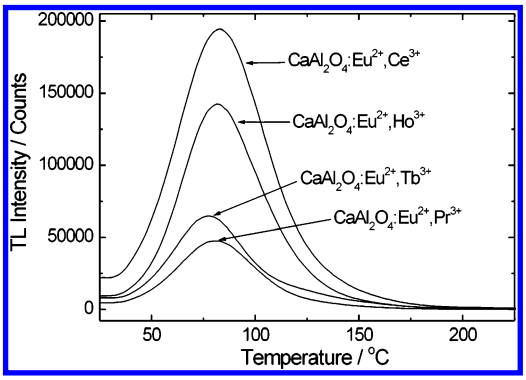


**Figure 6.** Thermoluminescence glow curves of $CaAl_2O_4:Eu^{2+},R^{3+}$ (R = Ce, Pr, Tb, and Ho; irradiation time, 10 s; heating rate, 5 °C $s^{-1}$).

structure (Figure 6), but with enhanced intensity when compared to that of $CaAl_2O_4:Eu^{2+}$. The shape of the main TL peak is now more symmetric. Though these codopants do not change significantly the main peak position, the $Tb^{3+}$-codoped material has the maximum shifted to a slightly lower temperature. The intensity of the high temperature tail has thus decreased or the main peak gained more intensity and hides completely the tail. These ions enhance slightly the persistent luminescence intensity but not much the lifetime. As a conclusion, they increase the number of the traps corresponding to the main TL peak, but not the deeper ones, which are important for the lengthening of the persistent luminescence. The $Pr^{3+}$ and $Ho^{3+}$ ions enhanced also the low-temperature TL whereas $Tb^{3+}$ and $Ce^{3+}$ had rather a negative effect.[24]

The $Nd^{3+}$, $Dy^{3+}$, and $Tm^{3+}$ ions enhance strongly the intensity of the high-temperature tail of the $CaAl_2O_4:Eu^{2+}$ glow curve (Figure 7). The $Dy^{3+}$-codoped material has a very broad TL peak structure with the first maximum at ca. 90 °C superimposed by even a stronger one at ca. 130 °C. The $Dy^{3+}$ ions created slightly too deep traps for efficient persistent luminescence and,

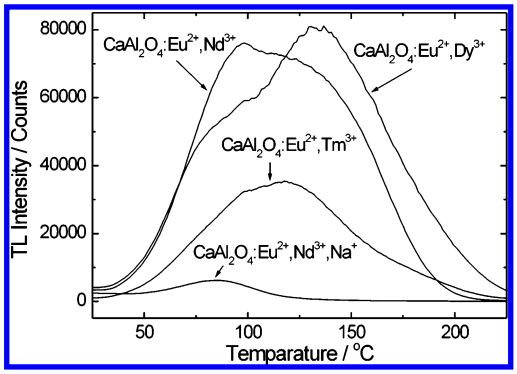


**Figure 7.** Thermoluminescence glow curves of $CaAl_2O_4:Eu^{2+},R^{3+}$ (R = Nd, Dy, Tm, and Na; irradiation time, 10 s; heating rate, 5 °C $s^{-1}$).

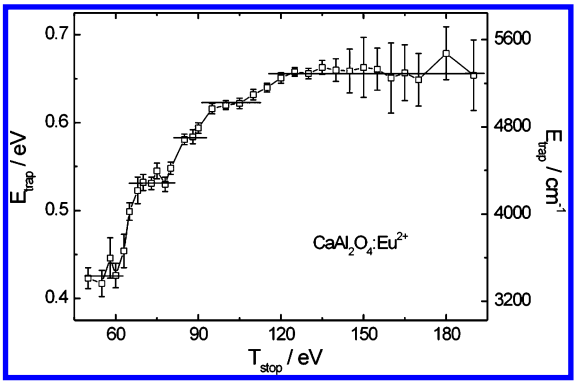


**Figure 8.** Trap depths of $CaAl_2O_4:Eu^{2+}$ estimated by the preheating and initial rise methods.

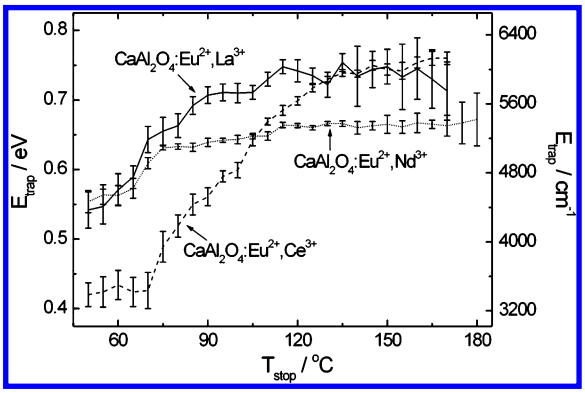


**Figure 9.** Trap depths of selected $CaAl_2O_4:Eu^{2+},R^{3+}$ (R = La, Ce, and Nd) estimated by the preheating and initial rise methods.

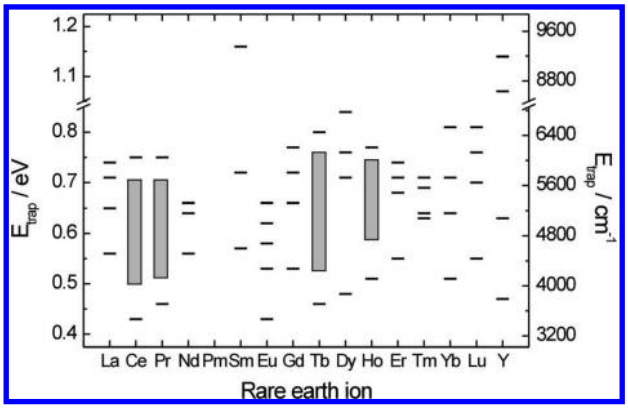


**Figure 10.** Effect of the $R^{3+}$ codoping on the trap depths of $CaAl_2O_4:Eu^{2+}$ (columns: continuously distributed energies).

on the other hand, too shallow ones as observed by the low-temperature TL measurements.[24] The glow curve obtained with $Nd^{3+}$ codoping has a very broad band between 40 and 200 °C peaking at ca. 100 °C and probably consisting of several TL peaks close to each other. $CaAl_2O_4:Eu^{2+},Tm^{3+}$ displays only one clear TL peak at ca. 120 °C, but the asymmetric shape of the peak suggests several overlapping maxima. $Nd^{3+}$ and $Tm^{3+}$ are the most efficient codopants to yield the intense and long-lasting persistent luminescence of $CaAl_2O_4:Eu^{2+},R^{3+}$, because they increase the number of the deep traps, corresponding to the high-temperature TL peaks.

**3.3. Thermoluminescence Kinetics and Fading.** The kinetics of the main TL peak in the $CaAl_2O_4:Eu^{2+}$ glow curve was studied by measuring the peak position as a function of the irradiation dose. The peak position was not observed to shift to lower temperatures with longer irradiation times. The absence of such a shift suggests first-order kinetics. On the other hand, when longer irradiation times were used (Figure 3), the intensity of the high temperature tail increased, compared to the main peak. In fact, the TL peak position seemed to move to slightly higher temperatures with longer irradiation times that cannot be explained by the simple first- or second-order kinetics. This kind of an effect has also been observed for the $CaSO_4:Dy^{3+}$ dosimetry materials.[32,33] The TL peak shift can be explained to be due to the different filling rates of the traps with similar energies. All $R^{3+}$-codoped $CaAl_2O_4:Eu^{2+}$ materials displayed a similar kind of behavior, too.

The main TL peak of the $CaAl_2O_4:Eu^{2+}$ glow curve was concluded to be responsible for the persistent luminescence at room temperature since when the material was stored for several hours in the dark prior to the TL measurement, the main peak was hardly observed (insert of Figure 3). The fading of the main TL peak was so fast that when the TL measurement was carried out 10 h after irradiation only the high temperature peak (corresponding to the tail) was observed. The intensity of the high temperature peak had also decreased indicating the bleaching of the deeper traps probably by tunneling. Since the main peak is hardly visible, the stepwise bleaching of the deep traps is not effective. The same kind of fading was observed for all $R^{3+}$-codoped aluminates. This observation unfortunately reveals that the use of these materials as conventional radiation detectors will be complicated because the detector should be stored at low temperatures in order to prevent fading. Alternatively, the fading time profile should be known.

**3.4. Trap Depths.** The different trap depths were derived from the glow curve of $CaAl_2O_4:Eu^{2+}$ with the aid of the preheating technique. Even the virtually simple main TL peak at ca. 80 °C corresponds to three traps with energies close to each other. The main TL peak region was found to correspond to ca. 0.42, 0.53, and 0.58 eV (3400, 4300, and 4700 $cm^{-1}$) deep traps by the initial rise method of the preheated glow curves (Figure 8). In addition, at least two traps with energies of 0.62 and 0.66 eV (5000 and 5300 $cm^{-1}$) were derived from the TL peaks at higher temperatures. The trap energies are very close to each other and even a continuous distribution of energies is possible.

All $R^{3+}$ ions seem to deepen the traps in $CaAl_2O_4:Eu^{2+}$ (Figures 9 and 10). The lowest energy traps (0.4−0.5 eV) of $CaAl_2O_4:Eu^{2+}$ seem to be missing in the $La^{3+}$-, $Gd^{3+}$-, $Er^{3+}$-, and $Lu^{3+}$-codoped materials; at least they cannot be derived from the glow curves. The main TL peak and the high temperature tail do not overlap so strongly, and thus the results obtained for the $La^{3+}$-, $Gd^{3+}$-, $Er^{3+}$-, and $Lu^{3+}$-codoped materials are more unambiguous. Several different traps could be derived in the wide energy range, 0.5−0.7 eV, for the $Ce^{3+}$-, $Pr^{3+}$-, $Tb^{3+}$-, and $Ho^{3+}$-codoped materials (Figures 9 and 10).

Alternatively, the nearly linear shape of the trap depth curve suggests continuously distributed trap energies. The most efficient codopants ($Nd^{3+}$ and $Tm^{3+}$) to obtain persistent luminescence seem to have more closely connected trap energies in the ranges of 0.55−0.65 and 0.62−0.72 eV, respectively. This can induce stronger interaction between the traps. The persistent luminescence may be explained by thermal release and retrapping of the charge carrier(s) from deeper traps via shallow ones to the recombination center. The low-temperature TL peaks can, however, be hidden by the high-temperature ones and cannot be detected by the preheating and initial rise methods.

As a conclusion, the $R^{3+}$ ions deepened the shallow traps in $CaAl_2O_4:Eu^{2+}$ by 0.01−0.2 eV and the deep ones by 0.01−0.4 eV. This means that the lifetimes of the charge carriers in the shallow and deep traps of $CaAl_2O_4:Eu^{2+},R^{3+}$ are ca. 1.5−2500 and 1.5−($6 \times 10^6$) times longer, respectively, than those of $CaAl_2O_4:Eu^{2+}$, if a constant frequency factor is assumed (eq 2). The trap densities (i.e., TL intensity) are, however, decreased for most $R^{3+}$-codoped materials. Therefore, the trap depth is not the only important parameter when the persistent luminescence properties are estimated.

The initial rise method gave several traps for each material. The trap depths were not the same as those obtained by the heating rate method[14] based on the shift of the TL peaks as a function of the heating rate. In fact, not even the same trends were obtained. It should thus be concluded that the simple methods, as the heating rate technique, are not the best ones to estimate the trap depths in the aluminates due to the strong overlap of the TL peaks. However, the initial rise method has some drawbacks, too. For example, the temperature range used in the analysis as well as the background signal of the glow curve may affect the assessment of trap depths. The curve fitting was also considered but the strong TL peak overlap found by the preheating technique discouraged the use of the fitting procedure. The challenge in the curve fitting was to find physically reliable trapping parameters, since the curve deconvolution can give several mathematically good solutions that have nothing to do with the real TL process.[34,35] The detailed comparison of the different methods for the evaluation of the trap parameters (trap depths, frequency factors and lifetimes) is out of the scope of this work and will be presented elsewhere.

**3.5. Trapping Mechanisms. 3.5.1. Mechanisms Proposed Earlier.** In the early studies of persistent luminescence, the $Eu^{2+}$ ion has been assumed to act both as an electron trap as well as a luminescent center and the $R^{3+}$ ion as a hole trap in the $MAl_2O_4:Eu^{2+},R^{3+}$ materials; see, e.g., refs 10−13. The mechanisms proposed involve a highly doubtful process, the reduction of $Eu^{2+}$ to $Eu^{+}$. The reduction of $Eu^{2+}$ and, to a lesser extent, the oxidation of $R^{3+}$ is impossible under the near UV and visible excitation due to lack of sufficient energy. The presence of $Eu^{+}$ or $Dy^{4+}$ have not been observed by the X-ray absorption measurements of $SrAl_2O_4:Eu^{2+},Dy^{3+}$, either.[36] More recently, the $R^{3+}$ ions have been proposed to act as electron traps in $SrAl_2O_4:Eu^{2+},R^{3+}$.[16] The mechanism is based on the photoionization of $Eu^{2+}$ and trapping of the electron via conduction band by the $R^{3+}$ ion. The photoionization of $Eu^{2+}$ was found plausible, since the 5d levels were found to be located partly in the conduction band.[16] The problem of the both mechanisms above is that the $Eu^{2+}$-doped materials yield strong persistent luminescence alone and no $R^{3+}$ codoping is really necessary—though feasible in some cases. Thus, other trapping centers and mechanisms have to be considered.

The oxygen ($V_O$) and calcium ($V_{Ca}$) vacancies were proposed to act as trapping levels for electrons and holes, respectively,

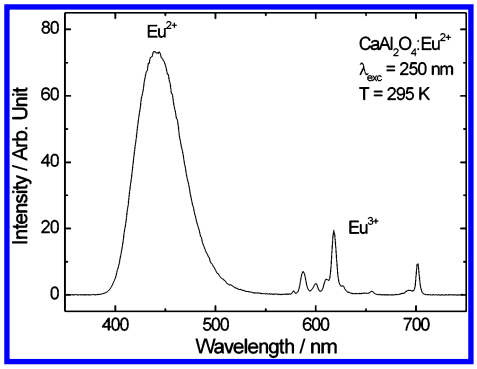


**Figure 11.** Time-resolved UV excited luminescence spectrum of $CaAl_2O_4:Eu^{2+}$ at room temperature.

in the $Eu^{2+}$-doped aluminates.[14,37] Trapping was presented to be followed by thermal bleaching and an energy transfer to the $Eu^{2+}$ ion from an electron−hole recombination process. Oxygen vacancies have also been reported to act as electron traps in many storage phosphors.[38,39] Because the $R^{3+}$ ions ($R_M$) replace the $M^{2+}$ ions in the $MAl_2O_4$ materials,[40,41] the natural consequence is the formation of charge compensating lattice defects, e.g., $M^{2+}$ vacancies. Permanent interstitial oxygens are not presumably formed because of the reducing preparation conditions. Rather, oxygen vacancies may be formed. The $M^{2+}$ vacancies are also formed by $Eu^{2+}$ doping, since some $Eu^{3+}$ ions are always present in the materials even if the reducing preparation conditions have been used. This is indicated by the $Eu^{3+}$ luminescence (Figure 11). The $M^{2+}$ vacancies are also formed without $R^{3+}$ codoping. Another rather different approach may be considered, too. The surface composition of $CaAl_2O_4$ has been found to be nonstoichiometric since the surface was found to be enriched in aluminum.[42] This kind of behavior would lead not only to the deficiency of calcium and oxygen on the surface but also to the deficiency of aluminum deeper in the material, too. The identification of the lattice defects was not, however, completed.[42] These kinds of defects that are formed on the surface of the bulky material may also act as trapping levels and take part in the luminescence processes.

Another mechanism based on the $Eu^{2+}$ photoionization and an electron trapping to oxygen vacancies has been presented for the persistent luminescence of $SrAl_2O_4:Eu^{2+},Dy^{3+}$.[17] The $Dy^{3+}$ ion has been believed to move electron density to an oxygen vacancy and thus stabilize oxygen vacancies in the vicinity of $Eu^{2+}$. This is based on the supposition that the lower is the ionization potential of the cation, the greater is the ability of the cation to attract (and thus stabilize) an oxygen vacancy. $Dy^{3+}$ would thus reinforce the attraction of $Eu^{2+}$, since the ionization potential of $Dy^{3+}$ is lower than that of $Sr^{2+}$. The experimental data presented[17] to prove or support this mechanism are, however, insufficient and mostly based on private communications and results with restricted access. There are thus several different proposals for the persistent luminescence mechanisms. Possible trapping levels should be described and discussed more precisely as it is done in the following chapters.

**3.5.2. Ability of $R^{3+}$ to Act as Traps.** The physical effect of the $R^{3+}$ codoping seems to be the suppression of TL intensity since $La^{3+}$, $Gd^{3+}$, $Lu^{3+}$, and $Y^{3+}$, which have very high ionization and 4f → 5d energies,[43,44] quench the intensity. Therefore, it might be concluded that the formed $M^{2+}$ vacancies (i.e., hole traps) are not, after all, the only important factors for the persistent luminescence. The oxidation and reduction (i.e., the ability to trap a hole or an electron, respectively) of the $R^{3+}$ ions should thus be considered in more detail. This can be

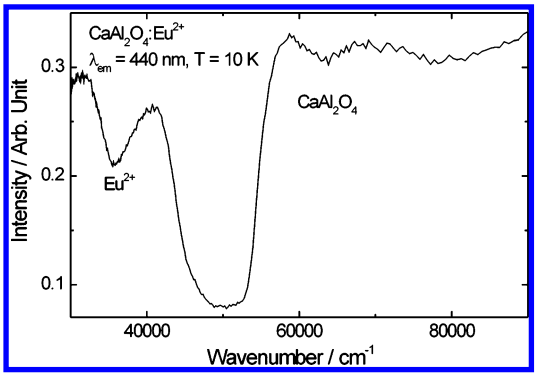


**Figure 12.** Luminescence excitation spectrum of $CaAl_2O_4:Eu^{2+}$ at VUV/UV region at 10 K.

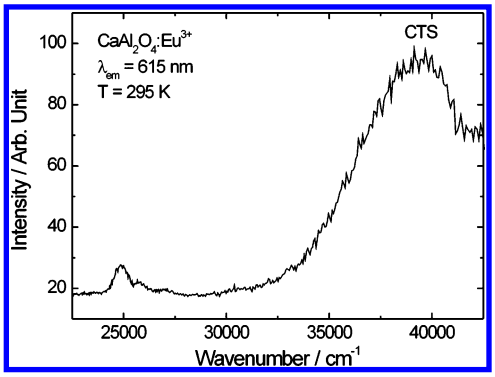


**Figure 13.** Luminescence excitation spectrum of $CaAl_2O_4:Eu^{3+}$ at room temperature.

done, if the location of the $R^{3+}$ and $R^{2+}$ energy levels relative to the valence and conduction bands of the host lattice is known.

The location of the $R^{3+}$ and $R^{2+}$ energy levels in the band gap of $CaAl_2O_4$ can be estimated by using the method developed by P. Dorenbos (eqs 5 and 6).[25,26] The band gap of $CaAl_2O_4$ can be estimated as ca. 60 000 $cm^{-1}$ (7.4 eV) from the VUV excitation spectrum (Figure 12). The band gap energy is normally ca. 4000 $cm^{-1}$ (0.5 eV) higher than the fundamental absorption edge due to the exciton creation energy.[27] The 4f ground energy level of all $R^{3+}$ ions can be located vis-à-vis the host band structure, if the 4f ground level of one $R^{3+}$ ion is known. In the case of $CaAl_2O_4$, the location of the 4f ground level of $Ce^{3+}$ is approximately known based on the data on the luminescence from the lowest 5d level at 413 nm (24 200 $cm^{-1}$, 3.0 eV).[45] The further observation based on photoconduction measurements, that the 5d levels of the $Ce^{3+}$ ion are partly located in the conduction band, is also needed. The 4f ground level of the $Ce^{3+}$ ion was then located at 8900−11300 $cm^{-1}$ (1.1−1.4 eV) above the valence band. The band gap energy was, however, underestimated (46 800 $cm^{-1}$, 5.8 eV).[45] In the present work, the 4f ground level of $Ce^{3+}$ is therefore located at 22 100−24 500 $cm^{-1}$ (2.7−3.0 eV) above the valence band. The 4f ground levels of most $R^{3+}$ ions (excluding Ce, Pr, Tb, and Dy) are thus located in the valence band of $CaAl_2O_4$ (see chapter 2.5.). The 413 nm emission has been explained to be due to the $Ce^{3+}$ ion occupying a six-coordinated site.[45] The $Ce^{3+}$ ions in the other two sites, six- and nine-coordinated, have been found to have luminescence bands at 392 and 325 nm, respectively. There is almost a perfect match between the ionic radius of $Ce^{3+}$ (CN = 9: 1.196 and CN = 6: 1.01 Å) and $Ca^{2+}$ (CN = 9: 1.18 and CN = 6: 1.00 Å).[46] Some bands may, however, be due to the $Ce^{3+}$ ions with charge compensation defects. On the basis of the three possible sites, band asymmetry and charge compensation, the locations of the 4f ground levels of the $R^{3+}$ ions are not yet completely clear. They can be located even deeper in the valence band or/and the 5d levels closer to the conduction band. In the present work, the 413 nm emission of $Ce^{3+}$ is used for the energy level construction since it has been observed to be the strongest and has been measured with the best precision.[45]

The 4f ground levels of the $R^{2+}$ ions should be located in the forbidden gap or in the conduction band, since the ground level of one $R^{2+}$ is always higher than that of the same $R^{3+}$. The 4f ground levels of the $R^{2+}$ ions can be located if the charge-transfer energy (from ligand to the $R^{3+}$ ion) of one $R^{3+}$ ion is known, as explained earlier. In the case of $CaAl_2O_4$, the maximum of the O(2p)−$Eu^{3+}$ charge-transfer absorption band (Figure 13) is observed at ca. 39 500 $cm^{-1}$ (4.9 eV). The 4f ground level of $Eu^{2+}$ is thus located ca. 20 500 $cm^{-1}$ (2.5 eV)

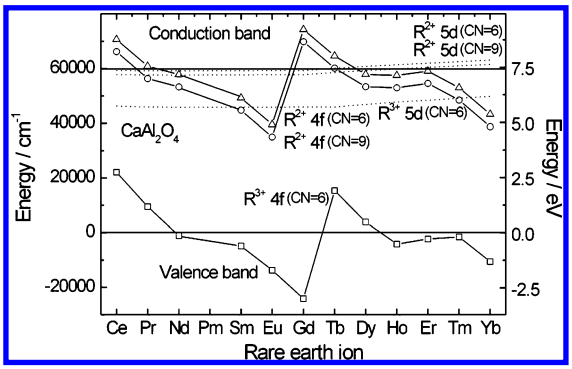


**Figure 14.** 4f and 5d ground energy level schemes of the $R^{3+}$ and $R^{2+}$ ions in $CaAl_2O_4$ estimated by the Dorenbos method.[25,26]

below the conduction band. Since the luminescence band of $Eu^{2+}$ is observed at 440 nm (22 700 $cm^{-1}$, 2.8 eV), the lowest 5d level should locate in the conduction band. This is not possible, since the $Eu^{2+}$ luminescence should be quenched in that case. Therefore, it can be concluded that the CT band observed is due to a $Eu^{3+}$ ion in a site different from that of the $Eu^{2+}$ ion. $Eu^{2+}$ locates preferably in the nine-coordinated $Ca^{2+}$ site,[40,41] but $Eu^{3+}$ may also locate in the two six-coordinated sites due to the smaller ionic radius (CN = 9, $Ca^{2+}$ = 1.18 Å, $Eu^{2+}$ = 1.30 Å, and $Eu^{3+}$ = 1.12 Å; CN = 6, $Ca^{2+}$ = 1.00 Å, $Eu^{2+}$ = 1.17 Å, and $Eu^{3+}$ = 0.947 Å [46]). The CT band can be used to locate the 4f ground levels of the $R^{2+}$ ions in the six-coordinated site. The luminescence band of the six-coordinated $Eu^{2+}$ is estimated (eq 7) to be found at ca. 505 nm (19 800 $cm^{-1}$, 2.5 eV) that locates the lowest 5d level very near the bottom of the conduction band. The 4f and 5d energy level locations of the nine-coordinated $Eu^{2+}$ can be estimated with the aid of the observation that no $Yb^{2+}$ luminescence has been found in $CaAl_2O_4:Yb^{2+}$.[47] All 5d levels of $Yb^{3+}$ are thus located in the conduction band. The lowest 5d level of the nine-coordinated $Eu^{2+}$ is then located ca. 2300 $cm^{-1}$ (0.3 eV) below the bottom of the conduction band, but the higher 5d levels are in the conduction band. The 4f ground level of the nine-coordinated $Eu^{2+}$ is then located ca. 25 000 $cm^{-1}$ (3.1 eV) below the conduction band. The location of the $Eu^{2+}$ 4f ground level is not completely certain, since the environments of $Eu^{2+}$ and $Eu^{3+}$ are never identical due to the vicinity of charge compensation defects caused by the $Eu^{3+}$ ion in a divalent site.

The energy level schemes (Figure 14) deserve some remarks of their utility. First, they indicate that only a few rare earths (Ce, Pr, Tb, and Dy) can be stable in the tetravalent form in $CaAl_2O_4$. In addition, the energy level schemes indicate also that most rare earths (excluding Ce, Gd, and perhaps Tb) can be in the divalent state in $CaAl_2O_4$. These remarks are of importance when different trapping schemes are considered later.

No direct correlation could be found between the TL results of $CaAl_2O_4:Eu^{2+},R^{3+}$ and the $R^{3+}$ or $R^{2+}$ ion ground energy level locations (Figure 14). This is in contradiction with the Dorenbos proposal[25,26] according to which the ground level positions of $R^{3+}$ and $R^{2+}$ in the forbidden gap may directly explain the different persistent luminescence properties of the $R^{3+}$-codoped materials. According to that model, the ability of a $R^{3+}$ ion to act as a hole trap may be estimated from the energy difference between the top of the valence band and the 4f ground level of the $R^{3+}$ ion. On the other hand, the ability of $R^{3+}$ ion to act as an electron trap may be estimated from the energy difference between the bottom of the conduction band (if an electron is first raised to the conduction band from the valence band or from an impurity ion) and the 4f ground level of the $R^{2+}$ ion.

The 4f ground level location of $R^{2+}$ could be related partly to the TL results for $CaAl_2O_4:Eu^{2+},R^{3+}$ (i.e., $R^{3+}$ would act as electron traps), since the ground levels of $Sm^{2+}$ and $Yb^{2+}$ are located at low energy in the forbidden gap; i.e., stable electron traps should be expected. Indeed, stable traps with $Sm^{3+}$ and $Yb^{3+}$ codoping are observed in this work in the TL glow curves. Other $R^{3+}$ ions, however, show that the model is not perfect; e.g., $Er^{3+}$ should have an effect similar to $Nd^{3+}$ and $Dy^{3+}$, but $Er^{3+}$ creates very shallow traps[24] and $Nd^{3+}$ and $Dy^{3+}$ deeper ones as observed in this work. The $R^{3+}$ ions acting directly as hole traps seem to offer no plausible explanation, since the ground levels of most $R^{3+}$ ions are located in the valence band.

One reason for the fact that no correlation between the TL results and the energy level locations of the rare earth ions is observed might be the deviations in the theoretical model, since it relies heavily on the data obtained for only a few rare earth ions ($Ce^{3+}$, $Pr^{3+}$, $Tb^{3+}$, $Eu^{2+}$, $Yb^{2+}$, $Sm^{2+}$).[25,29] The data for the remaining rare earth ions are mainly based on special materials (e.g., fluorides) and approximations. Because of the broad band character of the 4f → 5d (and 5d → 4f) transitions, even reading the position of the band can easily cause deviations up to 1500 $cm^{-1}$ (0.2 eV). In the case of the excitation spectra, the position should be read at the low energy side of the $^2D$ ($5d^1$) band due to coupling of the 5d to 4f levels (e.g., $Eu^{2+}$: $4f^6[^7F_{0-6}]$ splits the $5d^1$ excited levels each into seven multiplets).[48] In many cases, approximations should be done, because the coupling cannot be observed if the 5d levels are located near the conduction band. This problem will lead to a shift of the whole energy level location curve of rare earths, however. Finally, in the $CaAl_2O_4$ host, the $R^{3+}$ ions may favor different $Ca^{2+}$ sites; i.e., the larger ions ($La^{3+}-Sm^{3+}$) favor the nine-coordinated site and the smaller ones the six-coordinated sites. The $R^{3+}$ ion can even occupy all three sites. These different sites offer a very probable explanation for the deviation between the model and the TL results. The $R^{3+}$ ions may also form segregated phases. The effect of the $R^{3+}$ codoping would be more easy to study in a material where there is only one site with a good size match for $R^{3+}$ and $R^{2+}$.

**3.5.3. Role of Lattice Defects.** There are 12 oxygen sites in the $CaAl_2O_4$ lattice.[49] The many oxygen sites (and vacancies) in $CaAl_2O_4$ may offer an explanation to the dense trap energy distribution, i.e., closely overlapping TL peaks. In addition, similar to MgO and $Al_2O_3$, two kinds of electron traps are possible: one electron ($F^+$ center) or two electrons (F center) trapped into an oxygen vacancy.[50] The release of an electron from an oxygen vacancy seems thus to be the crucial (i.e., rate determining) step in the TL process. There are only three $Ca^{2+}$ sites in the lattice,[49] and the trap energy distribution cannot be explained as well by the slightly different hole traps, because more than three traps were derived with the aid of preheating method. However, both the electron and hole traps can be detected with the aid of thermoluminescence.

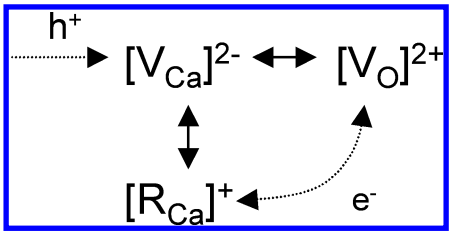


**Figure 15.** Proposed defect aggregate formed in $CaAl_2O_4:Eu^{2+},R^{3+}$.

The creation of the calcium vacancies by $R^{3+}$ codoping is well probable. However, they seem not to be of equal importance since all $R^{3+}$ ions do not enhance the persistent luminescence. Calcium vacancies can be important defects in creating aggregates with the oxygen vacancy and the $[R_{Ca}]^+$ ion. The oxygen vacancy and $R^{3+}$ in $Ca^{2+}$ site are both positively charged relative to the environment and can trap electrons. On the other hand, calcium vacancy is negatively charged and can trap a hole as well as aggregate with $V_O$ or/and $[R_{Ca}]^+$ (Figure 15). $V_O$ and $[R_{Ca}]^+$ would repulse each other without $V_{Ca}$.

The aggregation of lattice defects is a usual phenomenon in solid state.[51] The Mössbauer results showed[37] that even the $Eu^{2+}$ ions form aggregates in $CaAl_2O_4$, though there is no need due to the charge compensation defects with $Eu^{2+}$ doping. A size mismatch between $Ca^{2+}$ and $Eu^{2+}$ may initiate this aggregation.

The effect of the $R^{3+}$ ions on the oxygen vacancies should be considered, too. If an electron is transferred from the trap (i.e., an oxygen vacancy close to the $R^{3+}$ ion) to the $R^{3+}$ ion, the $R^{2+}$ ion (or $R^{3+}-e^-$ entity) could be formed. New TL peaks would then be observed. $Tm^{3+}$ (and $Nd^{3+}$) may act in this way, but $Sm^{3+}$ and $Yb^{3+}$ are, at least partly, reduced to the divalent state during the preparation of the materials. On the other hand, the effect of $Nd^{3+}$ is removed by $Na^+$ codoping (Figure 7). If $Nd^{3+}$ acts as an electron trap, $Na^+$ codoping should not affect the trapping process. This suggests that $Nd^{3+}$ does not directly act as a trap, but $Na^+$ removes the calcium vacancies created by $Nd^{3+}$, since one mono- and one trivalent codoping ion together balance two divalent host cations. Without $V_{Ca}$, the distance between $V_O$ and $Nd^{3+}$ is probably too long for an effective electron transfer. The $Sm^{2+}$ and $Yb^{2+}$ ions might have similar an effect as $Na^+$. They are partly divalent already and they can fill $V_{Ca}$. On the other hand, $Sm^{3+}$ and $Yb^{3+}$ can act as stable electron traps (i.e., 4f ground levels well below the bottom of the conduction band), and high temperature is needed to free an electron from them.

It is still unclear why different $R^{3+}$ ions do not behave similarly. The same aggregates should be formed in every case, excluding $Sm^{3+}$ and $Yb^{3+}$. Therefore, the ability to interact with charged traps and charge carriers must differ. The explanation might be the different reduction potentials of the $R^{3+}$ ions. The shape of the reduction potential curve of the $R^{3+}$ ions is similar to the 4f ground level curve of $R^{2+}$ (Figure 14). The most stable $R^{3+}$ ions (e.g., $La^{3+}$, $Gd^{3+}$, $Lu^{3+}$) have high potentials and the most readily reduced ones ($Eu^{3+}$, $Yb^{3+}$, $Sm^{3+}$) low potentials. In the $CaAl_2O_4:Eu^{2+},R^{3+}$ lattice, the $R^{2+}$ 4f ground level of stable $R^{3+}$ ions ($La^{3+}$, $Gd^{3+}$, $Lu^{3+}$) can be found in the conduction band (Figure 14) indicating the instability of the divalent state. The stable $R^{3+}$ ions can form aggregates with vacancies, but do not interact with the trapped electrons. Therefore, the electron freed from $V_O$ would not be trapped to $R^{3+}$ and the original trap is not stabilized by all $R^{3+}$ ions. On the other hand, all $R^{3+}$ ions suppress also the UV excited

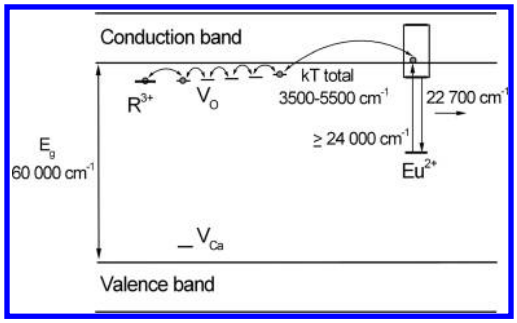


**Figure 16.** Proposed persistent luminescence mechanism for $CaAl_2O_4$:$Eu^{2+}$,$R^{3+}$ showing the possible trapping processes of electrons.

luminescence of $CaAl_2O_4$:$Eu^{2+}$ [14] that may be explained by the increasing probability of the nonradiative transitions. Therefore, the $R^{3+}$ ions, which cannot act as traps, suppress also the persistent luminescence. The $R^{3+}$ ions whose reduction potential value can be found in the middle of the curve (i.e., $Nd^{3+}$, $Dy^{3+}$, $Ho^{3+}$, $Er^{3+}$, $Tm^{3+}$) should have a similar effect on the persistent luminescence. Unfortunately, this is not the case. Therefore, there must be other criteria, too. Such could be the size of the $R^{3+}$ ion, which decreases quite smoothly from $La^{3+}$ (CN = 9: 1.21 Å) to $Lu^{3+}$ (CN = 9: 1.032 Å).[46] A strong electrostatic interaction occurs between the $R^{3+}$ ion and $e^-$. The Coulomb's law shows that the electrostatic energy of attraction increases when the interionic distance decreases. The electrostatic interaction of $Nd^{3+}$ with $e^-$ would thus be relatively weaker than, e.g., that of $Ho^{3+}$ or $Er^{3+}$. However, it is still impossible to explain in a quantitative manner the different behavior of, e.g., the $Dy^{3+}$, $Ho^{3+}$, and $Er^{3+}$ ions. It can be concluded that the effect of the $R^{3+}$ codoping seems to be composed of several factors. The small differences in different factors will finally lead to the large differences observed in the efficiency of persistent luminescence.

**3.5.4. New Mechanism for Persistent Luminescence.** On the basis of the results obtained in this and previous works,[14,24,37] a new persistent luminescence mechanism is proposed (Figure 16). The electrons are first excited from the 4f ground level of $Eu^{2+}$ to the 5d levels by the UV ($\geq$24 000 $cm^{-1}$) radiation. Because the 5d levels are partly in the conduction band of $CaAl_2O_4$, some electrons escape to the conduction band with the aid of thermal energy (i.e., lattice vibrations). Since the lifetimes of the $4f^65d^1 \rightarrow 4f^7$ transition and the lattice vibrations are of order of $10^{-6}$ and $10^{-12}$ s, respectively, there is enough time for the electron to escape. $Eu^{2+}$ stays now as $Eu^{3+}$ (or $Eu^{2+}-h^+$). The electron is trapped from the conduction band to an oxygen vacancy. The electron can migrate from one trap to another with the aid of acquiring (or releasing) thermal energy and also to the aggregated $R^{3+}$ ions forming $R^{2+}$ (or $R^{3+}-e^-$), which will prolong the persistent luminescence lifetime. The tunneling mechanism for the electron transfer is possible as inferred by the fading of thermoluminescence (insert of Figure 3). The reverse process from the traps via conduction band (or directly by tunneling) to the 5d levels of $Eu^{2+}-h^+$ produces the relaxation of the electron back to the ground level of $Eu^{2+}$ and persistent luminescence is observed.

Alternatively, the hole created to $Eu^{2+}-h^+$ by the electron escape may be trapped, too. The possible hole traps are the calcium vacancies and/or the $R^{3+}$ ions. However, only $Ce^{3+}$, $Pr^{3+}$, and $Tb^{3+}$ (and perhaps $Dy^{3+}$) may trap holes as indicated earlier. These ions do not fit well to the model presented above (Figure 16). They enhance the persistent luminescence but cannot trap electrons, because the $R^{2+}$ 4f ground levels can be found in (or near to) the conduction band. The recombination of the trapped electron and hole followed by an energy transfer to $Eu^{2+}$ would complete the persistent luminescence process. The location of the calcium vacancies in relation to the band structure of $CaAl_2O_4$ is, however, uncertain. They can only be supposed to locate near to the top of the valence band.

Holes have been previously reported to be the charge carriers in $MAl_2O_4$:$Eu^{2+}$,$R^{3+}$ based on the Hall effect[52] and photoconductivity[4] measurements, but as pointed out later,[16] those results do not provide evidence solid enough. The results obtained in this work suggest that the electrons are the main charge carriers in the persistent luminescence mechanism. The incoherent charge carrier results[4,52] might be understood, if the tunneling of electrons from traps to $Eu^{2+}$ occurs since in that case, the conducting species should be detected neither in the conduction (electrons) nor the valence (holes) band. If both the electrons and holes are trapped, the ambiguous charge carrier results would be expected.

## 4. Conclusions

The seemingly simple TL glow curve of $CaAl_2O_4$:$Eu^{2+}$ peaking at ca. 80 °C was observed to correspond to the several traps. All $R^{3+}$ ions did not have the same effect on the thermoluminescence properties of $CaAl_2O_4$:$Eu^{2+}$. A direct correlation was found between the persistent luminescence and thermoluminescence intensity of $CaAl_2O_4$:$Eu^{2+}$,$R^{3+}$. The $Nd^{3+}$ and $Tm^{3+}$ ions, which enhance the intensity of the high-temperature TL peaks, form the most suitable traps for intense and long-lasting persistent luminescence. The trap depths were estimated with the aid of the preheating and initial rise methods. The trap depths were affected by $R^{3+}$ codoping but not as much as the TL intensity. No clear correlation was found between the trap depths and the $R^{3+}$ or $R^{2+}$ ground energy level locations estimated by the Dorenbos method in $CaAl_2O_4$. This suggests that the traps are more complex than the simple charge transfer to (or from) the $R^{3+}$ ions.

A new persistent luminescence mechanism is proposed based on the photoionization of an electron from the 5d levels of $Eu^{2+}$ to the conduction band followed by the electron trapping to an oxygen vacancy. The close location of the 5d levels of $Eu^{2+}$ to the conduction band of $CaAl_2O_4$ makes the photoionization possible. The migration of the electron from one trap to another and also to the aggregated $R^{3+}$ ions forming $R^{2+}$ (or $R^{3+}-e^-$) then occurs. The reverse process from traps to $Eu^{2+}$ will produce the persistent luminescence. The ability of the $R^{3+}$ ions to trap electrons is probably based on the different reduction potentials and size of the $R^{3+}$ ions. Hole trapping to a calcium vacancy and/or the $R^{3+}$ ion may also occur. The mechanism presented can also explain why $Na^+$, $Sm^{3+}$, and $Yb^{3+}$ suppress the persistent luminescence. Other $Eu^{2+}$- and $R^{3+}$-doped aluminate and silicate materials are studied at the moment to confirm the role of the $R^{3+}$ codoping on the persistent luminescence.

**Acknowledgment.** This work was supported financially by the University of Turku and the Academy of Finland as well as the Graduate School of Materials Research (Turku, Finland). Mr. K. O. Eskola (Dating Laboratory, University of Helsinki, Helsinki, Finland), Prof. J.-C. Krupa (Institut de Physique Nucléaire, Orsay, France) and Prof. H. von Seggern (Department of Materials Science, Darmstadt University of Technology, Darmstadt, Germany) are acknowledged for the TL, VUV/UV, and time-resolved luminescence measurements, respectively. Useful discussions with Dr. F. Pellé (ENSCP, Paris, France) are acknowledged. Some of the rare earth oxides used in this work were provided by Rhôdia S.A. (Aubervilliers, France).

## References and Notes

(1) Blasse, G.; Grabmaier, B. C. *Luminescent Materials*; Springer: Berlin, Germany, 1994; pp 65−66.

(2) Murayama, Y. In *Phosphor Handbook*; Shionoya, S., Yen, W. M., Eds.; CRC Press: Boca Raton, FL, 1999; pp 651−658.

(3) Murayama, Y.; Takeuchi, N.; Aoki, Y.; Matsuzawa, T. U.S. Patent 5,424,006, 1995.

(4) Matsuzawa, T.; Aoki, Y.; Takeuchi, N.; Murayama, Y. *J. Electrochem. Soc.* **1996**, *143*, 2670−2673.

(5) Katsumata, T.; Nabae, T.; Sasajima, K.; Komuro, S.; Morikawa, T. *J. Electrochem. Soc.* **1997**, *144*, L243−L245.

(6) Katsumata, T.; Nabae, T.; Sasajima, K.; Matsuzawa, T. *J. Cryst. Growth* **1998**, *183*, 361−365.

(7) Katsumata, T.; Nabae, T.; Sasajima, K.; Komuro, S.; Morikawa, T. *J. Am. Ceram. Soc.* **1998**, *81*, 413−416.

(8) Sakai, R.; Katsumata, T.; Komuro, S.; Morikawa, T. *J. Lumin.* **1999**, *85*, 149−154.

(9) Tsutai, I.; Kamimura, T.; Kato, K.; Kaneko, F.; Shinbo, K.; Ohta, M.; Kawakami, T. *Electron. Eng. Jpn* **2000**, *132*, 7−14.

(10) Nakazawa, E.; Mochida, T. *J. Lumin.* **1997**, *72−74*, 236−237.

(11) Yamamoto, H.; Matsuzawa, T. *J. Lumin.* **1997**, *72−74*, 287−289.

(12) Jia, W.; Yuan, H.; Lu, L.; Liu, H.; Yen, W. M. *J. Lumin.* **1998**, *76&77*, 424−428.

(13) Kato, K.; Tsutai, I.; Kamimura, T.; Kaneko, F.; Shinbo, K.; Ohta, M.; Kawakami, T. *J. Lumin.* **1999**, *82*, 213−220.

(14) Aitasalo, T.; Dereń, P.; Hölsä, J.; Jungner, H.; Krupa, J.-C.; Lastusaari, M.; Legendziewicz, J.; Niittykoski, J.; Stręk, W. *J. Solid State Chem.* **2003**, *171*, 114−122.

(15) Nag, A.; Kutty, T. R. N. *Mater. Res. Bull.* **2004**, *39*, 331−342.

(16) Dorenbos, P. *J. Electrochem. Soc.* **2005**, *152*, H107−H110.

(17) Clabau, F.; Rocquefelte, X.; Jobic, S.; Deniard, P.; Whangbo, M.-H.; Garcia, A.; Le Mercier, T. *Chem. Mater.* **2005**, *17*, 3904−3912.

(18) Kowatari, M.; Koyama, D.; Satoh, Y.; Iinuma, K.; Uchida, S. *Nucl. Instrum. Methods Phys. Res. A* **2002**, *480*, 431−439.

(19) Xu, C.-N.; Watanabe, T.; Akiyama, M.; Zheng, X.-G. *Appl. Phys. Lett.* **1999**, *74*, 2414−2416.

(20) Xu, C.-N.; Zheng, X.-G.; Akiyama, M.; Nonaka, K.; Watanabe, T. *Appl. Phys. Lett.* **2000**, *76*, 179−181.

(21) Akiyama, M.; Xu, C.-N.; Liu, Y.; Nonaka, K.; Watanabe, T. *J. Lumin.* **2002**, *97*, 13−18.

(22) Aizawa, H.; Katsumata, T.; Takahashi, J.; Matsunaga, K.; Komuro, S.; Morikawa, T.; Toba, E. *Electrochem. Solid-State Lett.* **2002**, *5*, H17−H19.

(23) McKeever, S. W. S. *Thermoluminescence of Solids*; Cambridge University Press: New York, USA, 1985; pp 64−87.

(24) Aitasalo, T.; Durygin, A.; Hölsä, J.; Lastusaari, M.; Niittykoski, J.; Suchocki, A. *J. Alloys Compd.* **2004**, *380*, 4−8.

(25) Dorenbos, P. *J. Phys.: Condens. Matter* **2003**, *15*, 8417−8434.

(26) Dorenbos, P. *J. Lumin.* **2004**, *108*, 301−305.

(27) Dorenbos, P. *J. Lumin.* **2005**, *111*, 89−104.

(28) Dorenbos, P. *J. Lumin.* **2003**, *104*, 239−260.

(29) Dorenbos, P. *J. Lumin.* **2000**, *91*, 155−176.

(30) Cao, X.; Dolg, M. *Chem. Phys. Lett.* **2001**, *349*, 489−495.

(31) Dorenbos, P. *J. Phys.: Condens. Matter* **2003**, *15*, 2645−2665.

(32) Lakshmanan, A. R. *Prog. Mater. Sci.* **1999**, *44*, 88−107.

(33) Jose, M. T.; Madhusoodanan, U.; Lakshmanan, A. R. *J. Phys. D: Appl. Phys.* **2001**, *34*, 717−721.

(34) Bos, A. J. J.; Piters, T. M.; Gómez Ros, J. M.; Delgado, A. *Radiat. Prot. Dosim.* **1993**, *47*, 473−477.

(35) Bos, A. J. J.; Piters, T. M.; Gómez Ros, J. M.; Delgado, A. *Radiat. Prot. Dosim.* **1994**, *51*, 257−264.

(36) Qiu, J.; Kawasaki, M.; Tanaka, K.; Shimizugawa, Y.; Hirao, K. *J. Phys. Chem. Solids* **1998**, *59*, 1521−1525.

(37) Hölsä, J.; Aitasalo, T.; Lastusaari, M.; Niittykoski, J.; Spano, G. *J. Alloys Compd.* **2004**, *374*, 56−59.

(38) Meijerink, A.; Schipper, W. J.; Blasse, G. *J. Phys. D: Appl. Phys.* **1991**, *24*, 997−1002.

(39) Kodama, N.; Takahashi, T.; Yamaga, M.; Tanii, Y.; Qiu, J.; Hirao, K. *Appl. Phys. Lett.* **1999**, *75*, 1715−1717.

(40) Nakamura, T.; Matsuzawa, T.; Rowlands, C. C.; Beltrán-López, V.; Smith, G. M.; Riedi, P. C. *J. Chem. Soc., Faraday Trans.* **1998**, *94*, 3009−3012.

(41) Nakamura, T.; Kaiya, K.; Takahashi, N.; Matsuzawa, T.; Ohta, M.; Rowlands, C. C.; Smith, G. M.; Riedi, P. C. *Phys. Chem. Chem. Phys.* **2001**, *3*, 1721−1723.

(42) Ball, M. C.; Marsh, C. M.; Simmons, R. E.; Sutherland, I.; Symons, M. C. R. *J. Mater. Sci.* **1988**, *23*, 1431−1435.

(43) Morss, L. S. *Chem. Rev.* **1976**, *76*, 827−841.

(44) Meyer, G. *Chem. Rev.* **1988**, *88*, 93−107.

(45) Jia, D.; Yen, W. M. *J. Electrochem. Soc.* **2003**, *150*, H61− H65.

(46) Shannon, R. D. *Acta Crystallogr. A* **1976**, *32*, 751−767.

(47) Lizzo, S.; Nagelvoort, E. P. K.; Erens, R.; Meijerink, A.; Blasse, G. *J. Phys. Chem. Solids* **1997**, *58*, 963−968.

(48) Dorenbos, P. *J. Phys.: Condens. Matter* **2003**, *15*, 575−594.

(49) Hörkner, W.; Müller-Buschbaum, H. K. *J. Inorg. Nucl. Chem.* **1976**, *38*, 983−984.

(50) Agullo-Lopez, F.; Catlow, C. R. A.; Townsend, P. D. *Point Defects in Materials*; Academic Press: London, U.K., 1988; pp 149−161.

(51) Henderson, B. *Defects in Crystalline Solids*; Edward Arnold: London, U.K., 1972; pp 2−9.

(52) Abbruscato, V. *J. Electrochem. Soc.* **1971**, *118*, 930−933.